Universal discrete Fourier optics RF photonic integrated circuit architecture

Trevor J. Hall and Mehedi Hasan*

Photonic Technology Laboratory, Centre for Research in Photonics, Advanced Research Complex, University of Ottawa, 25 Templeton Street, Ottawa, K1N 6N5, ON, Canada
mhasa067@uottawa.ca

Abstract: This paper describes a coherent electro-optic circuit architecture that generates a frequency comb consisting of N spatially separated orders using a generalised Mach-Zenhder interferometer (MZI) with its $N \times 1$ combiner replaced by an optical $N \times N$ Discrete Fourier Transform (DFT). Advantage may be taken of the tight optical path-length control, component and circuit symmetries and emerging trimming algorithms offered by photonic integration in any platform that offers linear electro-optic phase modulation such as $LiNbO_3$, silicon, III-V or hybrid technology. The circuit architecture subsumes all MZI-based RF photonic circuit architectures in the prior art given an appropriate choice of output port(s) and dimension N although the principal application envisaged is phase correlated subcarrier generation for all optical orthogonal frequency division multiplexing. A transfer matrix approach is used to model the operation of the architecture. The predictions of the model are validated by simulations performed using an industry standard software tool. Implementation is found to be practical.

OCIS codes: (170.1065) Acousto-optics; (230.2090) Electro-optical devices; (060.5625) Radio frequency photonics; (250.4110) Modulators; (070.2025) Discrete optical signal processing.

References and links

1. M. Reck, A. Zeilinger, H. J. Bernstein, and P. Bertani, "Experimental realization of any discrete unitary operator," Phys. Rev. Lett. **73**(1), 58–61 (1994).
2. J. Carolan, C. Harrold, C. Sparrow, E. Martín-López, N. J. Russell, J. W. Silverstone, P. J. Shadbolt, N. Matsuda, M. Oguma, M. Itoh, G. D. Marshall, M. G. Thompson, J. C. F. Matthews, T. Hashimoto, J. L. O'Brien, and A. Laing, "QUANTUM OPTICS. Universal linear optics," Science **349**(6249), 711–716 (2015).
3. D. A. B. Miller, "Perfect optics with imperfect components," Optica **2**(8), 747–750 (2015).
4. M. Izutsu, S. Shikama, and T. Sueta, "Integrated optical SSB modulator / frequency shifter," IEEE J. Quantum Electron. **17**(11), 2225–2227 (1981).
5. G. H. Smith, D. Novak, and Z. Ahmed, "Overcoming chromatic-dispersion effects in fiber-wireless systems incorporating external modulators," IEEE Trans. Microw. Theory Tech. **45**(8), 1410–1415 (1997).
6. A. Wen, M. Li, L. Shang, and Y. Chen, "A novel optical SSB modulation scheme with interfering harmonics suppressed for ROF transmission link," Opt. Laser Technol. **43**(7), 1061–1064 (2011).
7. C. W. Chow, C. H. Wang, C. H. Yeh, and S. Chi, "Analysis of the carrier-suppressed single-sideband modulators used to mitigate Rayleigh backscattering in carrier-distributed PON," Opt. Express **19**(11), 10973–10978 (2011).
8. M. Hasan, R. Maldonado-Basilio, and T. J. Hall, "Studies in an optical millimeter-wave generation scheme via two parallel dual-parallel Mach-Zehnder modulators," J. Mod. Opt. **62**(7), 581–583 (2015).
9. P.-T. Shih, J. Chen, C.-T. Lin, W.-J. Jiang, H.-S. Huang, P.-C. Peng, and S. Chi, "Optical millimeter-wave signal generation via frequency 12-tupling," J. Lightwave Technol. **28**(1), 71–78 (2010).
10. H. Yamazaki, T. Saida, T. Goh, S. Mino, M. Nagatani, H. Nosaka, and K. Murata, "Dual-carrier dual-polarization IQ modulator using a complementary frequency shifter," IEEE J. Sel. Top. Quantum Electron. **19**(6), 3400208 (2013).
11. R. Maldonado-Basilio, M. Hasan, R. Guemri, F. Lucarz, and T. J. Hall, "Generalized Mach–Zehnder interferometer architectures for radio frequency translation and multiplication: suppression of unwanted harmonics by design," Opt. Commun. **354**, 122–127 (2015).
12. M. Hasan, R. Maldonado-Basilio, and T. J. Hall, "Dual-function photonic integrated circuit for frequency octo-tupling or single-side-band modulation," Opt. Lett. **40**(11), 2501–2504 (2015).

#257715 Received 19 Jan 2016; revised 13 Mar 2016; accepted 15 Mar 2016; published 30 Mar 2016

13. R. Maldonado-Basilio, M. Hasan, H. Nikkhah, S. Abdul-Majid, R. Guemri, F. Lucarz, J.-L. de Bougrenet de la Tocnaye, and T. J. Hall, "Electro-optic up-conversion mixer amenable to photonic integration," J. Mod. Opt. **62**(17), 1405–1411 (2015).
14. Y. Ma, Q. Yang, Y. Tang, S. Chen, and W. Shieh, "1-Tb/s single-channel coherent optical OFDM transmission over 600-km SSMF fiber with subwavelength bandwidth access," Opt. Express **17**(11), 9421–9427 (2009).
15. T. Miwa and K. Takiguchi, "Integrated-optic OFDM signal multiplexer composed of optical IFFT circuit," Electron. Lett. **51**(6), 505–506 (2015).
16. K. Takiguchi, M. Oguma, H. Takahashi, and A. Mori, "Integrated-optic eight-channel OFDM demultiplexer and its demonstration with 160 Gbit/s signal reception," Electron. Lett. **46**(8), 575–576 (2010).
17. K. Takiguchi, T. Kitoh, A. Mori, M. Oguma, and H. Takahashi, "Integrated-optic OFDM demultiplexer using slab star coupler based optical DFT circuit," 36th European Conference and Exhibition on Optical Communication (ECOC), Torino, 2010, pp. 1–3.
18. W. Li, X. Liang, W. Ma, T. Zhou, B. Huang, and D. Liu, "A planar waveguide optical discrete Fourier transformer design for 160 Gb/s all-optical OFDM systems," Opt. Fiber Technol. **16**(1), 5–11 (2010).
19. A. G. Kirk, A. K. Powell, and T. J. Hall, "A Generalisation of the Error Diffusion Method for Binary Computer Generated Hologram Design," Opt. Commun. **92**(1-3), 12–18 (1992).
20. A. E. Siegman, "Fiber Fourier optics," Opt. Lett. **26**(16), 1215–1217 (2001).
21. M. E. Marhic, "Discrete Fourier transforms by single-mode star networks," Opt. Lett. **12**(1), 63–65 (1987).
22. G. Cincotti, "Generalized fiber Fourier optics," Opt. Lett. **36**(12), 2321–2323 (2011).
23. G. Cincotti, "What else can an AWG do?" Opt. Express **20**(26), B288–B298 (2012).
24. J. Zhou, "All-optical discrete Fourier transform based on multimode interference couplers," IEEE Photonics Technol. Lett. **22**(15), 1093–1095 (2010).
25. J. Zhou, "Realization of discrete Fourier transform and inverse discrete Fourier transform on one single multimode interference coupler," IEEE Photonics Technol. Lett. **23**(5), 302–304 (2011).
26. D. A. B. Miller, "Perfect optics with imperfect components Perfect optics with imperfect components: supplementary material," http://dx.doi.org/10.1364/optica.2.000747.s001.
27. S. Abdul-Majid, R. Maldonado-Basilio, C. Lei, H. Awad, I. Hasan, W. N. Ye, and T. J. Hall, "Performance analysis of a photonic integrated interferometer circuit based on silicon-on-insulator," Opt. Quantum Electron. **47**(7), 1965–1971 (2015).
28. M. Hasan, R. Guemri, R. Maldonado-Basilio, F. Lucarz, J.-L. de Bougrenet de la Tocnaye, and T. Hall, "Theoretical analysis and modeling of a photonic integrated circuit for frequency 8-tupled and 24-tupled millimeter wave signal generation," Opt. Lett. **39**(24), 6950–6953 (2014).
29. R. Halir, P. J. Bock, P. Cheben, A. Ortega-Monux, C. Alonso-Ramos, J. H. Schmid, J. Lapointe, D. Xu, J. G. Wanguemert-Perez, I. Molina-Fernandez, and S. Janz, "Waveguide sub-wavelength structures: a review of principles and applications," Laser Photonics Rev. **9**(1), 25–49 (2015).
30. A. Natarajan, A. Komijani, X. Guan, A. Babakhani, and A. Hajimiri, "A 77-GHz phased-array transceiver with on-chip antennas in silicon: transmitter and local LO-path phase shifting," IEEE J. Solid-State Circuits **41**(12), 2807–2819 (2006).
31. A. Chiba, T. Kawanishi, T. Sakamoto, K. Higuma, K. Takada, and M. Izutsu, "Low-crosstalk balanced bridge interferometric-type optical switch for optical signal routing," IEEE J. Sel. Top. Quantum Electron. **19**(6), 3400307 (2013).
32. D. Marpaung, C. Roeloffzen, R. Heideman, A. Leinse, S. Sales, and J. Capmany, "Integrated microwave photonics," Laser Photonics Rev. **7**(4), 506–538 (2013).
33. R. Slavík, S. G. Farwell, M. J. Wale, and D. J. Richardson, "Compact Optical Comb Generator Using InP Tunable Laser and Push-Pull Modulator," IEEE Photonics Technol. Lett. **27**(2), 217–220 (2015).
34. H. Subbaraman, X. Xu, A. Hosseini, X. Zhang, Y. Zhang, D. Kwong, and R. T. Chen, "Recent advances in silicon-based passive and active optical interconnects," Opt. Express **23**(3), 2487–2510 (2015).
35. X. Zhang, B. Lee, C. Lin, A. X. Wang, A. Hosseini, and R. T. Chen, "Highly Linear Broadband Optical Modulator Based on Electro-Optic Polymer," IEEE Photonics J. **4**(6), 2214–2228 (2012).
36. P. Rabiei, J. Ma, S. Khan, J. Chiles, and S. Fathpour, "Heterogeneous lithium niobate photonics on silicon substrates," Opt. Express **21**(21), 25573–25581 (2013).
37. W. H. P. Pernice, C. Xiong, F. J. Walker, and H. X. Tang, "Design of a silicon integrated electro-optic modulator using ferroelectric $BaTiO_3$ films," IEEE Photonics Technol. Lett. **26**(13), 1344–1347 (2014).
38. J. Li, Z. Liu, Y. Tu, S.-T. Ho, I. W. Jung, L. E. Ocola, and B. W. Wessels, "Photonic crystal waveguide electro-optic modulator with a wide bandwidth," J. Lightwave Technol. **31**(10), 1601–1607 (2013).
39. D. Korn, R. Palmer, H. Yu, P. C. Schindler, L. Alloatti, M. Baier, R. Schmogrow, W. Bogaerts, S. K. Selvaraja, G. Lepage, M. Pantouvaki, J. M. D. Wouters, P. Verheyen, J. Van Campenhout, B. Chen, R. Baets, P. Absil, R. Dinu, C. Koos, W. Freude, and J. Leuthold, "Silicon-organic hybrid (SOH) IQ modulator using the linear electro-optic effect for transmitting 16QAM at 112 Gbit/s," Opt. Express **21**(11), 13219–13227 (2013).
40. M. J. R. Heck, J. F. Bauters, M. L. Davenport, J. K. Doylend, S. Jain, G. Kurczveil, S. Srinivasan, Y. Tang, and J. E. Bowers, "Hybrid silicon photonic integrated circuit technology," IEEE J. Sel. Top. Quantum Electron. **19**(4), 6100117 (2013).
41. J. W. Goodman, *Introduction to Fourier Optics,* 3rd ed. (Roberts & Company Publishers, 2005).

#257715 Received 19 Jan 2016; revised 13 Mar 2016; accepted 15 Mar 2016; published 30 Mar 2016

1. Introduction

With the transition from incoherent to coherent optical systems a revolution in optical communications technology is in progress. At long last, rather than field intensity, information is now conveyed by the amplitudes of the components of the vector field (polarisation, magnitude and phase). It is theoretically possible to construct a coherent optical circuit with sufficient versatility to implement any possible linear operation. This follows because any loss-less linear optical circuit is described by a unitary operator, and a specific array of basic two-mode operations is mathematically sufficient to implement any unitary operator [1]. Many advanced optical functions, including fundamental tests of quantum mechanics and quantum technologies; and arbitrary linear optical processors for communications could be implemented using meshes of Mach–Zehnder interferometers [2]. Ironically, the physical layer functions required by optical communications networks are more easily expressed but far more challenging to implement within a coherent optical rather than an incoherent optical conceptual framework. The reason is the extreme short wavelength of light (~1 μm), which demands path length tolerances in the region of ~1 nm if the phase is to be controlled within a complex circuit architecture; performance can be severely degraded by small imperfections of optical components. Fortunately, another revolution in optical component technology is in progress with a transition from discrete components interconnected by optical fibre to integrated components interconnected by planar optical waveguides within a photonic integrated circuit. Integration brings tight dimensional tolerances and, more significantly, extremely tight relative dimensional tolerances. The latter enables circuit designers to ameliorate impairments by making use of component symmetries that are robust to photonic integrated circuit fabrication errors but impractical with discrete components. Moreover, methodologies for trimming circuit parameters to achieve perfect optics with imperfect components are emerging [3].

Meshes of Mach–Zehnder interferometers (MZI) feature widely in the field of radio frequency (RF) photonics. There has been a plethora of publications [4–9] over the last decade that have described essentially the same Generalized Mach-Zehnder Interferometer (GMZI) circuit architecture: a $1 \times N$ splitter directly interconnected to a $N \times 1$ combiner via an array of N electro-optic $LiNbO_3$-based phase modulators, each circuit adapted to particular design goals. The applications have generally been to: in- and quadrature- (IQ) phase modulation, single sideband modulation, electro-optic frequency up-conversion [4–7]; radio frequency (RF) multiplication [8,9]; and multiple carrier generation [10]. The difference between the circuits proposed have largely concerned variations of the static optical and electrical phase shifts required or the implementation of an equivalent circuit using standard Mach-Zehnder modulators (MZM) rather than individual phase-modulators (PM) as the basic building brick. A generalized design methodology that determines the parameters of the architecture required to meet specified design objectives such as the suppression of unwanted intermodulation products has been reported in [11]. It has also been shown [12,13], how to use the intrinsic phase relations between the ports of splitters and combiners and specifically multi-mode interference (MMI) couplers to implement the static optical phase shifts required by these circuits, thereby avoiding the need to apply static DC bias to the electro-optic modulators and the associated drift issues that otherwise require complex stabilization circuitry. This paper describes and analyses a coherent electro-optic circuit architecture that generates N spatially distinct phase-correlated harmonically related carriers using a GMZI with its $N \times 1$ combiner replaced by an $N \times N$ optical Discrete Fourier Transform (DFT). Advantage may be taken of the tight optical path-length control, component and circuit symmetries and emerging trimming algorithms offered by photonic integration. The architecture subsumes all MZI-based architectures in the prior art given an appropriate choice of output port(s) and dimension N although the principal application envisaged is phase

#257715 Received 19 Jan 2016; revised 13 Mar 2016; accepted 15 Mar 2016; published 30 Mar 2016

correlated subcarrier generation for next generation optical transmission systems beyond 1Terabit / second using all optical orthogonal frequency division multiplexing.

Super-channel transmission has already been reported experimentally [14–18] to facilitate high data rates. One common demerit in these demonstrations is that all subcarriers exit from the same port by means of optical comb generation. Hence, an optical de-multiplexing filter is needed to separate these subcarriers individually so that they can be modulated. However, the limited tuning range and temperature sensitivity of an optical de-multiplexing filter makes the system implementation complicated and reduces the system performance. The design of a complementary phase shifter capable of generating two spatially separated subcarriers has been reported [10] but, with ever increasing demand for bandwidth, a circuit design capable of generating more than two spatially separated subcarriers is required for near future optical systems.

The paper is organized as follows. First, to provide intuition, acousto-optic diffraction in the Raman-Nath regime is considered within the framework of classical Fourier optics. This motivates a discretization that replaces the acousto-optic modulator by a set of waveguide phase-modulators excited by a waveguide splitter; electrically driven from the same RF source but with a progressive phase increment; and with light from their egress port processed by an optical DFT network. A transfer matrix analysis of this architecture then shows that it operates as expected with carriers with frequency shift $q\omega_{RF}$ emitted from output port q modulo N. The options for the implementation of the DFT network are considered and a specific example based on MMIs elaborated for $N = 4$. Layout considerations result in re-ordering and consolidation of elements that can remove any obvious connection to a travelling phase modulation wave and Fresnel diffraction. The analysis is then verified by simulation both in the ideal case and in the presence of impairments. The paper closes with a discussion of implementation feasibility and a summary of the main results.

2. Classical Raman-Nath diffraction

As a consequence of Fresnel diffraction, an ideal thin lens forms, in its real focal plane, the Fourier transform of the field in its front focal plane. A point source, represented by a Dirac delta distribution at the origin of the front focal plane, is thereby transformed to a constant amplitude field in the real focal plane. Hence, in Fig. 1, the spherical wave emanating from the point source at the origin in the front focal plane of lens L_1 is collimated into a plane wave propagating along the optical axis to provide a uniform amplitude field in its rear focal plane. Similarly, lens L_2 forms, in its rear focal plane, the Fourier transform of the field in its front focal plane. Consequently, the Fourier transform of the field transmitted by the acousto-optic modulator (AOM) is formed at the screen. In the absence of the AOM, lenses L_1 and L_2 ideally form a stigmatic image of the point source on the screen. In practice, the ideal image is convolved by a point-spread function caused by the finite apertures of the system's components. An acoustic wave induces within the aperture of the AOM a travelling phase grating via the elasto-optic effect. In the Raman-Nath regime the AOM behaves as a thin transmittance and the image on the screen splits into multiple diffraction orders.

The optical field a at the exit of the AOM due to a plane acoustic wave propagating in the x-direction transverse to the optical axis is given by:

$$a(x) = \exp[i\eta \cos(\Omega t - Kx)]. \tag{1}$$

where $\eta = \Delta nkl$ is the peak optical phase change caused by the peak refractive index change Δn induced by the acoustic wave via the elasto-optic effect, $k = 2\pi/\lambda$ is the vacuum optical wavenumber, λ is the vacuum optical wavelength, l is the acousto-optic interaction length, Ω is the frequency of the acoustic wave $K = 2\pi/\Lambda$ is the acoustic wavenumber, Λ is the acoustic wavelength, and t is time. Invoking the Jacobi-Angier expansion:

#257715 Received 19 Jan 2016; revised 13 Mar 2016; accepted 15 Mar 2016; published 30 Mar 2016

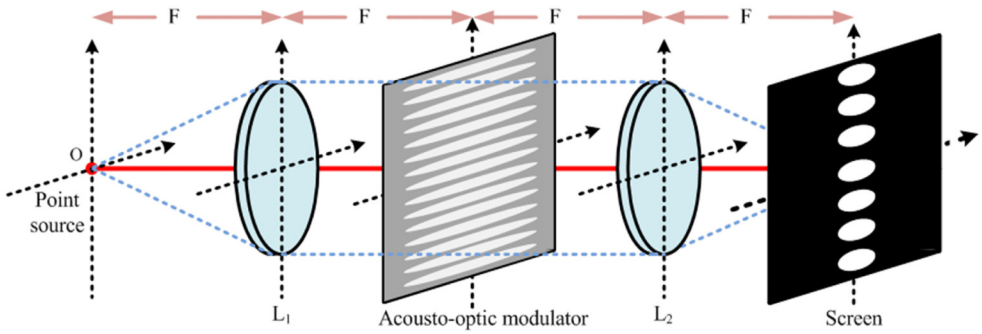

Fig. 1. A classical free-space coherent optical system for the observation of continuous Raman-Nath diffraction. Lens L_1 provides the acousto-optic modulator with uniform collimated illumination. The acousto-optic modulator (AOM) generates a travelling refractive index wave within its aperture. Lens L_2 provides the Fourier transform of the light transmitted by the AOM at the screen where Raman-Nath diffraction orders are observed.

$$\exp(i\eta\cos\theta)=\sum_{q=-\infty}^{\infty} i^q J_q(\eta)\exp(iq\theta). \tag{2}$$

yields:

$$a(x)=\sum_{q=-\infty}^{\infty} i^q J_q(\eta)\exp[iq(\Omega t-\mathrm{K}x)]. \tag{3}$$

where J_q is the Bessel function of the first kind of order q. The lens L_2 forms, in its rear focal plane, the Fourier transform $\hat{a}$ of the field a in its front focal plane:

$$\hat{a}=\frac{1}{2\pi}\int_{-\infty}^{\infty} a(x)\exp(-i\xi x)dx. \tag{4}$$

where the spatial frequency variable ξ is mapped into a transverse spatial co-ordinate by the optical system. Performing the Fourier transform one obtains an infinite train of Dirac distributions located at $\xi=-qK$ with mass $i^q J_q(\eta)\exp(iq\Omega t)$:

$$\hat{a}(x)=\sum_{q=-\infty}^{\infty} i^q J_q(\eta)\exp(iq\Omega t)\delta(\xi+q\mathrm{K})]. \tag{5}$$

This is the familiar Raman-Nath diffraction pattern with the temporal frequency of each order Doppler shifted by $q\Omega$. The different temporal frequency components of the field are thereby spatially separated.

Suppose, rather than plane wave-illumination, multiple beamlets (for example generated by a Fourier array generator [19]) sample the travelling phase grating on a regular lattice with period Λ/N then the spatial spectrum is replicated on a regular lattice with lattice constant NK. The Raman-Nath orders are thereby superimposed into equivalence classes corresponding to order q modulo N. A single period of the spectral orders is then related to a single period of the sampled phase grating by a DFT.

2.1 Discrete Raman-Nath diffraction

Pursuing the observation in the preceding section, consider the circuit shown in Fig. 2 consisting of a $1 \times N$ uniform light splitter that excites an array of N identical electro-optic waveguide phase modulators with outputs combined by a passive coherent optical network

#257715 Received 19 Jan 2016; revised 13 Mar 2016; accepted 15 Mar 2016; published 30 Mar 2016

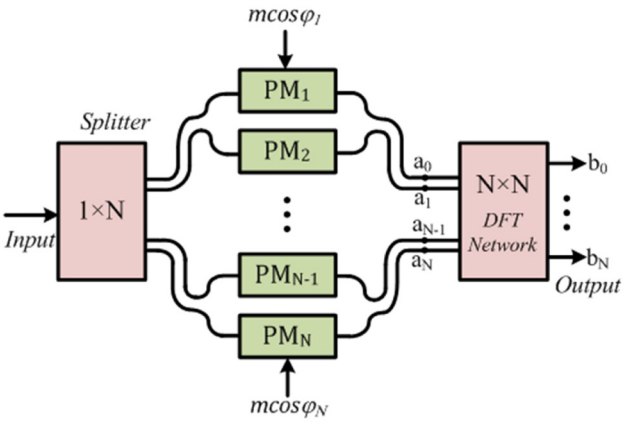

Fig. 2. Schematic diagram of an array of N phase modulators in parallel between a $1 \times N$ splitter and $N \times N$ DFT network. PM: phase modulator; DFT: discrete Fourier transform.

that emits light from its output ports with complex amplitudes b_q equal to the DFT of the complex amplitudes a_p of the light entering its input ports, where p and q are integers that index the ports:

$$b_q = \frac{1}{\sqrt{N}} \sum_{p=0}^{N-1} a_p \exp(-ipq\, 2\pi/N). \tag{6}$$

Let each phase modulator be driven by an RF source of angular frequency Ω with a progressive phase shift with increment $2\pi/N$:

$$v_p = v_{RF} \cos[\Omega t + p(2\pi/N)]. \tag{7}$$

For light of unit amplitude at the input of the splitter, the complex amplitude a_p of the light exiting the phase modulators is:

$$\begin{aligned} a_p &= \frac{1}{\sqrt{N}} \exp(i\pi\, v_p / v_\pi) \\ &= \frac{1}{\sqrt{N}} \exp(i\pi\, v_{RF} / v_\pi) \cos[\Omega t + p(2\pi/N)]. \end{aligned} \tag{8}$$

where v_π is the half-wave voltage.

The output of the waveguide phase modulators may be interpreted as the discrete-space samples at $x = -pd$ of a single period of the continuous travelling phase function defined by Eq. (1) with a peak phase shift given by:

$$\eta = \pi \frac{v_{RF}}{v_\pi}. \tag{9}$$

and a spatial frequency of the periodic extension of a single period of the samples given by:

$$\mathrm{K} = \frac{2\pi}{\Lambda}; \qquad \Lambda = Nd. \tag{10}$$

where d is the sampling interval.

Substituting Eq. (8) into Eq. (6) and invoking the Jacobi-Angier expansion Eq. (2) yields:

#257715 Received 19 Jan 2016; revised 13 Mar 2016; accepted 15 Mar 2016; published 30 Mar 2016

$$b_q = \frac{1}{N}\sum_{p=0}^{N-1}\sum_{r=-\infty}^{\infty} i^r J_r(\eta)\exp(ir\Omega t)\exp[ip(r-q)2\pi/N]. \tag{11}$$

Re-ordering the summations to give:

$$b_q = \sum_{r=-\infty}^{\infty} i^r J_r(\eta)\exp(ir\Omega t)\frac{1}{\sqrt{N}}\sum_{p=0}^{N-1}\exp[ip(r-q)p\,2\pi/N]. \tag{12}$$

and noting:

$$\begin{aligned}\frac{1}{\sqrt{N}}\sum_{p=0}^{N-1}\exp[i(r-q)p\,2\pi/N] &= 0 \qquad r \neq q \mod N\\ \frac{1}{\sqrt{N}}\sum_{p=0}^{N-1}\exp[i(r-q)p\,2\pi/N] &= 1 \qquad r = q \mod N.\end{aligned} \tag{13}$$

yields the final result:

$$b_q = \sum_{s=-\infty}^{\infty} i^{(q+sN)} J_{(q+sN)}(\eta)\exp[i(q+sN)\Omega t]. \tag{14}$$

It can be observed that all carriers of order q modulo N exit output port q as anticipated in the preceding section. The operation of the circuit architecture in Fig. 2 may therefore be understood in terms of discretized Raman-Nath diffraction. The circuit architecture subsumes the RF photonic circuits in the prior art for radio frequency (RF) multiplication; in- and quadrature- (IQ-) phase modulation / single sideband modulation / electro-optic frequency up-conversion; and frequency comb-generation given an appropriate choice of output port(s) and phase-modulator dimension N as is listed in Table 1.

Table 1. Circuit Architecture Configurations

Function	Dimension	Port(s) used
IQ modulation, SSB & electro-optic frequency conversion	$N = 4$	$q = 1$ or N-1
$\times N$ RF frequency multiplication	$N = 2q$	q
Spatially separated carrier generation	N = desired number of carriers	all

3. Discrete Fourier optics

It is well established that a suitable combination of waveguides and couplers may implement an optical DFT. The foundation of discrete Fourier optics was established by a pioneering paper in which Siegman proposed [20] a simple optical scheme previously also reported by Marhic [21], to perform the DFT of a parallel input signal using only passive couplers and phase shifters. Following the Cooley-Tukey algorithm, the $N \times N$ DFT is recursively decomposed into $\log_2(N)$ stages of 2×2 DFT elements in parallel that are realized by 180° optical hybrids implemented as 2×2 couplers. Subsequently, Cincotti [22] proposed a decomposition into larger dimension $M \times M$ DFT elements that are realized by $(360/M)°$ optical hybrids. This is advantageous in reducing the wiring complexity and the number of waveguide cross-overs. The DFT elements may be implemented using star-couplers [23] or multimode interference (MMI) couplers augmented by static phase shift elements [24, 25]. It is possible to implement any linear transformation including the DFT using a mesh of Mach-Zehnder Interferometers (MZI) [26]. Star-couplers and MMI depend upon Fresnel diffraction in 'free-space' slab waveguide regions that is sampled at its boundaries by single-mode planar waveguides. Networks that employ these components retain a connection to classical Fourier

#257715 Received 19 Jan 2016; revised 13 Mar 2016; accepted 15 Mar 2016; published 30 Mar 2016

optics that becomes tenuous when only directional couplers are used. For illustrative purposes, a 4 × 4 DFT realized using 2 × 2 MMI is considered in this paper. Figure 3(a) shows a network that performs a 4 × 4 DFT composed of four 180°-optical hybrids described by the transfer matrix:

$$S = \frac{1}{\sqrt{2}}\begin{pmatrix} 1 & 1 \\ 1 & -1 \end{pmatrix}.$$

and a π/2 phase shift element described by the transfer function:

$$z^{-1} = \exp(-i\,\pi/2).$$

A 2 × 2 MMI 3dB coupler is described by the transfer matrix:

$$S_{MMI} = \frac{1}{\sqrt{2}}\begin{pmatrix} 1 & -i \\ -i & 1 \end{pmatrix} = \frac{1}{\sqrt{2}}\begin{pmatrix} 1 & 0 \\ 0 & -i \end{pmatrix}\begin{pmatrix} 1 & 1 \\ 1 & -1 \end{pmatrix}\begin{pmatrix} 1 & 0 \\ 0 & -i \end{pmatrix}.$$

Hence:

$$S = -\begin{pmatrix} -i & 0 \\ 0 & 1 \end{pmatrix} S_{MMI} \begin{pmatrix} -i & 0 \\ 0 & 1 \end{pmatrix}.$$

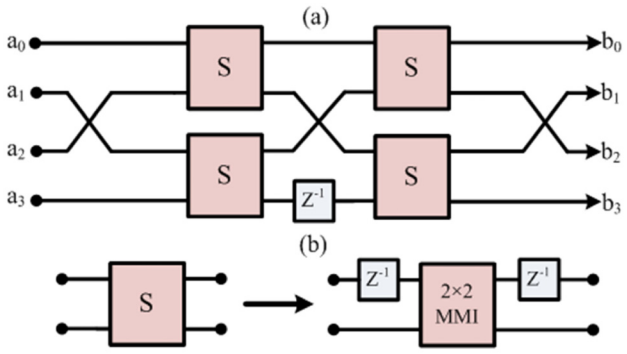

Fig. 3. (a) Schematic of a 4 × 4 DFT network; (b) realisation of *S* using a 2 × 2 MMI.

Consequently, up to a sign, the 180°-optical hybrids may be replaced by 2 × 2 MMI 3dB couplers with a π/2 phase shift element connected to its upper input and output port as shown in Fig. 3(b). Performing this substitution and eliminating any constant overall phase shifts yields the network shown in Fig. 4(a). The phase shift blocks at the front-end of the DFT network may be moved into the respective arm of the phase modulator array and placed at the front. The analysis in the preceding assumed that the 1 × *N* input splitter generated light at its egress ports of equal magnitude and phase. This may be achieved using a tree of 1 × 2 symmetric splitters. The cross-over at the front-end of the DFT network as shown in Fig. 4(a), may be removed by reordering the phase-modulators. This re-ordering has the effect of

#257715 Received 19 Jan 2016; revised 13 Mar 2016; accepted 15 Mar 2016; published 30 Mar 2016

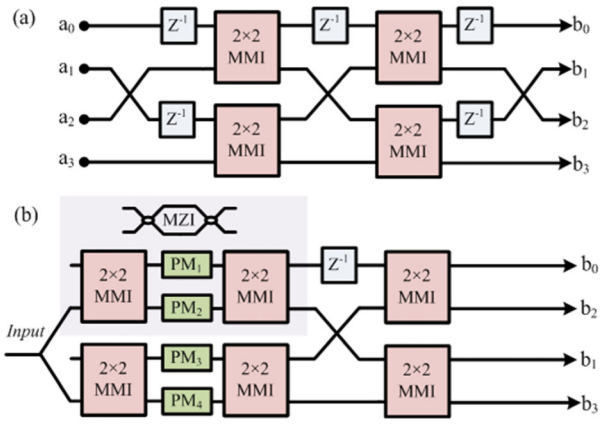

Fig. 4. (a) Schematic of a 4 × 4 DFT network using 2 × 2 MMI; (b) schematic of the complete circuit. The y-branch at the input represents a 1 × 2 symmetric coupler.

grouping the phase modulators into differentially driven pairs that form two Mach-Zehnder interferometers (MZI) statically biased by the phase-shift elements. The latter may be absorbed by replacing the 1 × 2 symmetric splitters on the egress side of the splitter tree by 2 × 2 MMI 3dB couplers. Moreover, in most applications the spatial location and absolute phase of an output is irrelevant which permits the cross-over and two delay elements on the output side of the DFT network to be removed. The final result is shown in Fig. 4(b).

4. Verification

The correct operation of the circuit is verified by simulation using an industry standard software tool (VPIphotonics). A continuous wave DFB laser set to operate at a vacuum wavelength 1550 nm with a power of 10 mW is used as an optical source. A 10 GHz RF source generating peak amplitude of $v_{RF} = 0.25v_{\pi}$ and an appropriate phase shift is applied to

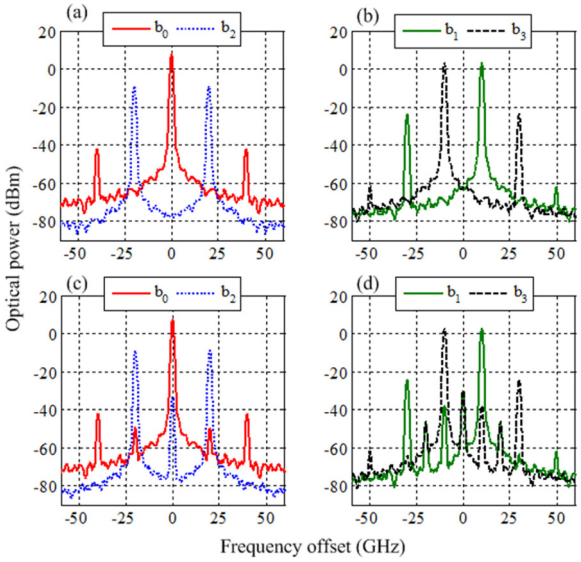

Fig. 5. Simulated optical spectrum, (a)-(b) without considering MMI errors due to fabrication tolerances; (c)-(d) with fabrication tolerances. A resolution bandwidth of 1 GHz is used for the optical spectrum analyzer. The optical noise floor is determined by the laser line-width, which is considered 200 kHz in this simulation.

#257715 Received 19 Jan 2016; revised 13 Mar 2016; accepted 15 Mar 2016; published 30 Mar 2016

the phase modulators. Figures 5(a) & (b) show the optical spectrum predicted by the simulation which verifies the theoretical predictions. The correct function of the circuit may deviate from ideal because of power imbalances and phase error between the ports of MMI due to fabrication errors and errors in the path length of the electrical waveguides that connects the RF source and phase modulator electrodes. It can be assume that all the components in a circuit will suffer similar impairments.

To account for the MMI tolerances, the S-matrix of an ideal MMI is perturbed to have 1° phase error and 0.70% power imbalances (well above simulated errors [27]) between the output ports and loaded for all the MMIs present in the circuit. The resultant optical spectra are shown in Figs. 5(c) & 5(d). Carrier break-through can be observed in the spectrum, thus limiting the overall performance. Nevertheless a minimum sub-harmonic suppression ratio (SHSR) of 24 dB and above can be achieved. It has been reported [28] that performance degrades more when RF drive phase error is considered as the RF phase error for a harmonic is a multiple equal to its order of the RF-drive phase error. Figure 6 shows the calculated SHSR for different phase error between the MZMs. It shows that other than the output at port

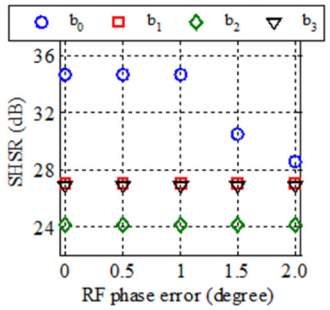

Fig. 6. Optical SHSR as a function of RF drive's phase errors between the MZMs.

b_O, all remain constant. A minimum SHSR of 24 dB and above is achieved. The optical phase errors can be reduced substantially over a broader bandwidth compared to a conventional MMI by the use of a sub-wavelength engineered MMI [29]. A linear summing amplifier can combine in-phase and quadrature phase RF signals to produce any desired RF phase shift and a CMOS implementation has been demonstrated operating at 77 GHz [30]. Co-integration of these RF phase-shifters with the optical circuitry will also avoid electrical phase shift errors and facilitates programmability and electrical trimming.

If required, additional small Mach-Zehnder interferometers may be integrated within the circuit to facilitate optical trimming [31] to improve the performance further, for example, by pursuing the ideas of Miller [3].The proposed circuit architecture may be implemented in any photonic integration platform [32] that can offer a linear electro-optic modulator. As many as 20 $LiNbO_3$ phase modulators hybridized to silica on silicon photonic light circuits by butt coupling have been demonstrated [10]. Continuous advances in performance of modulators based on InP [33], silicon [34], polymer [35]; and progress on hybrid integration of $LiNbO_3$ [36], $BaTi0_3$ [37,38], organic [39] thin-film electro-optic materials and III-V active devices [40] on silicon-on-insulator augurs very well that implementation is practical.

5. Conclusions

A coherent electro-optic circuit architecture that generates a frequency comb consisting of N spatially separated orders has been described. Intuition is provided by the space discretization of classical Raman-Nath diffraction. The circuit consists of a $1 \times N$ splitter that feeds light into a parallel array of electro-optic phase modulators each driven from the same RF source with a progressive phase shift with increment $2\pi/N$ with their phase modulated optical outputs processed by an $N \times N$ optical DFT. The circuit is not limited to a DFT and any linear optical

#257715 Received 19 Jan 2016; revised 13 Mar 2016; accepted 15 Mar 2016; published 30 Mar 2016

transformation may be substituted. Advantage may be taken of the tight optical path-length control, component and circuit symmetries and emerging trimming algorithms offered by photonic integration in any platform with a linear electro-optic phase modulator. The circuit subsumes many prior RF photonic circuit architectures given an appropriate choice of output port(s) and dimension *N*, although the principal application envisaged is phase correlated subcarrier generation. The predictions of a transfer matrix model of the circuit operation are validated by simulations performed using an industry standard software tool. Implementation is found to be practical. This suggests that free-space optical information processing systems [41] demonstrated in the past may find renewed application in discrete space form.

Acknowledgments

The authors acknowledge the Natural Sciences and Engineering Research Council of Canada (NSERC) for their support through a Strategic Project Grant STPGP 430176-12. Trevor J. Hall is grateful to the Canada Research Chair (CRC) Program for their support of his CRC-I in Photonic Network Technology.

#257715 Received 19 Jan 2016; revised 13 Mar 2016; accepted 15 Mar 2016; published 30 Mar 2016